ACS APPLIED MATERIALS & INTERFACES

Research Article

www.acsami.org

Enzyme-Specific Sensors via Aggregation of Charged *p*-Phenylene Ethynylenes

Eric H. Hill,[†,‡] Yue Zhang,[†] Deborah G. Evans,[‡] and David G. Whitten*[,†]

[†]Center for Biomedical Engineering, Department of Chemical and Biological Engineering, and [‡]The Nanoscience and Microsystems Engineering Program and Department of Chemistry and Chemical Biology, University of New Mexico, Albuquerque, New Mexico 87131-1341, United States

Supporting Information

ABSTRACT: Chemical and biological sensors are sought for their ability to detect enzymes as biomarkers for symptoms of various disorders, or the presence of chemical pollutants or poisons. *p*-Phenylene ethynylene oligomers with pendant charged groups have been recently shown to have ideal photophysical properties for sensing. In this study, one anionic and one cationic oligomer are combined with substrates that are susceptible to enzymatic degradation by phospholipases or acetylcholinesterases. The photophysical properties of the J-aggregated oligomers with the substrate are ideal for sensing, with fluorescence quantum yields of the sensors enhanced between 30 and 66 times compared to the oligomers without substrate. The phospholipase sensor was used to monitor the activity of phospholipase A1 and A2 and obtain kinetic information, though phospholipase C did not degrade the sensor. The acetylcholinesterase sensor was used to monitor enzyme activity and was also used to detect the inhibition of acetylcholinesterase by three different inhibitors. Phospholipase A2 is a biomarker for heart and circulatory disease, and acetylcholinesterase is a biomarker for Alzheimer's, and indicative of exposure to certain pesticides and nerve agents. This work shows that phenylene ethynylene oligomers can be tailored to enzyme-specific sensors by careful selection of substrates that induce formation of a molecular aggregate, and that the sensing of enzymes can be extended to enzyme kinetics and detection of inhibition. Furthermore, the aggregates were studied through all-atom molecular dynamics, providing a molecular-level view of the formation of the molecular aggregates and their structure.

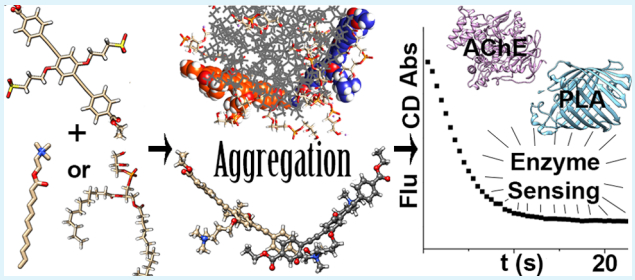

KEYWORDS: *enzyme sensing, chemical sensing, molecular aggregation, biosensing, biomarkers, fluorescence quenching*

INTRODUCTION

Chemical and biological sensors are of importance for detection of enzymes and their substrates, as either can serve as potential biomarkers for diseases, differentiating between normal and abnormal tissue, or for study of normal biological processes involved in activities such as exercise.[1−6] Cells or tissue that have become damaged or diseased tend to express different proteins than normal, which become very useful when it comes to diagnosing cardiovascular disease, cancer, Parkinson's Disease, and a plethora of other diseases.[7−9] This has been a burgeoning topic in healthcare research in the past decade, as advances in characterization methods have enabled accelerated discovery of new and known biomarkers in humans for a variety of tissue conditions and diseases.[6−9] Enzymes have been shown to be useful biomarkers in a variety of different tissue pathologies and diseases, and their ability to catalytically react with a substrate invites the design of chemical sensors that are able to detect these enzymes through exploiting the enzymes reaction with its substrate to induce a photophysical change.

Sensors for detection of enzyme activity have taken many forms. In recent years, much interest in inorganic materials for sensing has led to development of enzyme sensors based on materials such as graphene and carbon nanotubes.[10−12] Fluorescent organic molecules have been a mainstay of biological sensing techniques for decades, because of their ability to undergo changes in fluorescence upon binding to an analyte.[13−17] This has been commonly achieved through use of a conjugated organic molecule as a fluorophore, and recent studies by Kool and co-workers have highlighted the benefits of nucleic-acid based fluorescent sensors.[18] When considering the use of conjugated organic molecules for fluorescence sensing of an analyte, the two strategies that can be applied are either fluorescence quenching or enhancement. For detection of enzyme activity, a substrate can be used to induce either fluorescence quenching or unquenching that is reversed upon enzyme activity on the substrate.

Charged *p*-phenylene ethynylenes have been shown to be useful for their sensing activity resulting from their ability to form molecular aggregates or undergo conformational changes that give strong photophysical changes.[13,19−24] In earlier work by Schanze and co-workers, polymeric *p*-phenylene ethynylenes (PPEs) with anionic side chains were used to detect protease

Received: January 7, 2015
Accepted: February 20, 2015
Published: February 20, 2015

DOI: 10.1021/acsami.5b00185
ACS Appl. Mater. Interfaces 2015, 7, 5550−5560

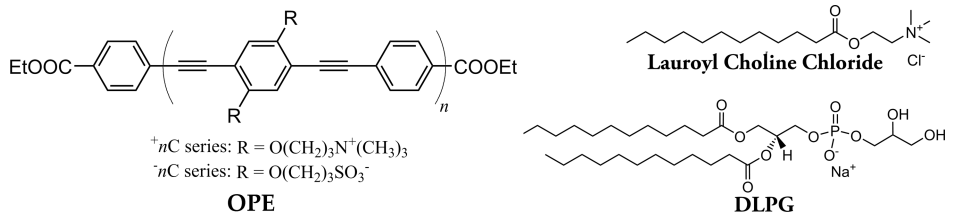

Figure 1. Carboxyester-terminated *p*-phenylene ethynylenes; cationic OPEs with n = 1, 2, and 3 and a single anionic OPE with n = 1.

and phospholipase C activity.[20] In the past several years, the development of monomers and oligomers of *p*-phenylene ethynylenes (OPEs) has given rise to a series of molecules with well-defined photophysical and biocidal properties.[19,21] They have been shown to form molecular aggregates on a variety of molecules and substrates, resulting in structurally different complexes depending on the shape of the molecule.[21−24] One particular class of these compounds with carboxyester terminal groups has very strong quenching of fluorescence in aqueous solution and makes a strong candidate for fluorescence quenching and unquenching assays.[24] The structure of this series of compounds is shown in Figure 1.

The previous study of these compounds showed that oppositely charged surfactants can induce the formation of molecular aggregates with strong photophysical changes, including a drastically enhanced fluorescence.[24] In order to achieve a sensor to detect the activity of an enzyme, the aggregation of the OPEs was induced by the substrate of the targeted enzyme. This provided enzyme specificity that would be useful when analyzing a complex mixture of enzymes.

The purpose of this study was to investigate the capability of these OPEs to detect the activity of enzymes that are implicated in disease or healthcare concerns. Phospholipase A2 has been shown to be a significant biomarker that implicates increased incidence of coronary heart disease and other cardiovascular diseases.[25−31] This is in part due to PLA2 inducing formation of small, dense low-density lipoprotein particles by modification of the circulating lipoproteins, and the hydrolysis products of PLA2 stiffening the arteries.[28−30] The activity of PLA2 is similar to that of PLA1, which cleaves the phospholipid on the other acyl chain. Phospholipase C (PLC), on the other hand, cleaves the phospholipid at the phosphate, releasing diacylglycerol as a product. PLA1 and PLA2 were both tested in this study, and the effect of PLC on the sensor was also monitored to compare with previous results with a PPE by Schanze and co-workers.[20] To form this sensor, a molecular aggregate was formed between a cationic, n = 2 OPE and the anionic lipid DLPG.

Acetylcholinesterase (AChE) is a critical enzyme for the central nervous system, as it is responsible for terminating nerve impulses via degradation of the neurotransmitter acetylcholine. This enzyme has profoundly widespread importance in healthcare and medicine for a variety of reasons. Exposure to nerve agents and pesticides causes the inhibition of AChE, inducing an increase in the AChE levels in the body which serves as a biomarker for pesticide or organophosphate exposure.[32−39] In recent years, AChE has also found use as a biomarker for neurodegenerative disorders such as Alzheimers Disease (AD), as affected areas of the brain such as lewy bodies have elevated AChE levels.[40−44] Although AD kills far fewer than heart disease (500 thousand versus 56 million yearly, worldwide), the increasing aging population has driven the number of people with AD to 5 million in the U.S. alone.

Because AD has no firm method of diagnosis and no cure, it is imperative to further develop strategies to detect and eliminate the neurofibrillary tangles and plaques which are hallmarks of the disease. To detect AChE activity, a sensor composed of the anionic OPE monomer OPE1-in a molecular aggregate with lauroyl choline (LaCh), was used. The photophysical properties of the sensors and the changes induced by enzyme activity were followed by UV−vis absorbance, fluorescence, and circular dichroism (CD) spectroscopy. Herein the carboxyester-terminated OPE are used to form enzyme sensors for two classes of enzymes that are disease biomarkers. The linear response of the phospholipase sensor to substrate concentration allowed for calculation of kinetic parameters of PLA1 and PLA2, whereas the AChE sensor was further used to detect the presence of AChE inhibitors. The results of this study will highlight the capabilities of this class of compounds for biosensing applications, and will advance the current state of healthcare research of detection of enzymes as potential biomarkers for disease or environmental pollution.

METHODS

Materials. −1C was synthesized as previously described by Tan and co-workers.[45] +2C was synthesized as previously reported by Tang and co-workers.[21] Both OPEs are light yellow solids, and readily dissolve in aqueous solution. Lauroyl choline chloride (Tokyo Chemical Industry Co.; Tokyo, Japan) was obtained as a solid powder and the container was stored under vacuum over desiccant. 1,2-dilauroyl-*sn*-glycero-3-phospho-(1′-rac-glycerol) (DLPG) (Avanti Polar Lipids, Alabaster, AL) was obtained as a lyophilized solid powder, and was dissolved in methanol and stored at −21 °C prior to use. Phospholipase A_1 (PLA1) from *Thermomyces lanuginosus* was obtained (Sigma-Aldrich, St. Louis, MO) as a liquid solution with a concentration of 10,000 Units/g. Phospholipase A_2 (PLA2) from *Crotalus adamanteus* venom was obtained as a lyophilized power with buffer salts at an activity of 320 U/mg (Worthington Biochemical, Lakewood, NJ). Acetylcholinesterase (AChE) from human erythrocytes was obtained as a pH 8.0 buffered solution with an activity of >500 U/mg (Sigma-Aldrich, St. Louis, MO). A unit (U) of PLA2 activity is measured as the amount of enzyme needed to release one micromole of titratable fatty acid per minute at pH 8.9 and 25 °C from lecithin emulsion. A unit of activity for PLA1 is defined the same, except at a pH of 7.5. AChE activity units are defined similarly, with one micromole of acetylthiocholine iodide hydrolyzed per minute at pH 7.4 and 37 °C. The AChE inhibitors Meptazinol HCl (3-(3-ethylhexahydro-1-methyl-1H-azepin-3-yl)-phenol hydrochloride), Itopride HCl (N-[[4-[2-(Dimethylamino)ethoxy]phenyl]methyl]-3,4-dimethoxy benzamidehydrochloride), and TAE-1 (2,2′,2′-[1,3,5-Triazine-2,4,6-triyltris(oxy-4,1-phenylenecarbonyloxy)]tris[N,N,N-trimethyl-ethanaminium tri-iodide) were obtained as solids (Sigma-Aldrich, St. Louis, MO). All solutions were prepared using filtered water with a resistivity of >18.2 MΩ cm (EMD Millipore, Billerica, MA), with a pH of 7.5.

Sample Preparation. A typical preparation of a −1C/LaCh sensor is given. In a quartz cuvette with stirring, 20 μL of 500 mM −1C is added to 1970 μL of water. After 15−30 s of mixing, 10 μL of a

DOI: 10.1021/acsami.5b00185
ACS Appl. Mater. Interfaces 2015, 7, 5550−5560

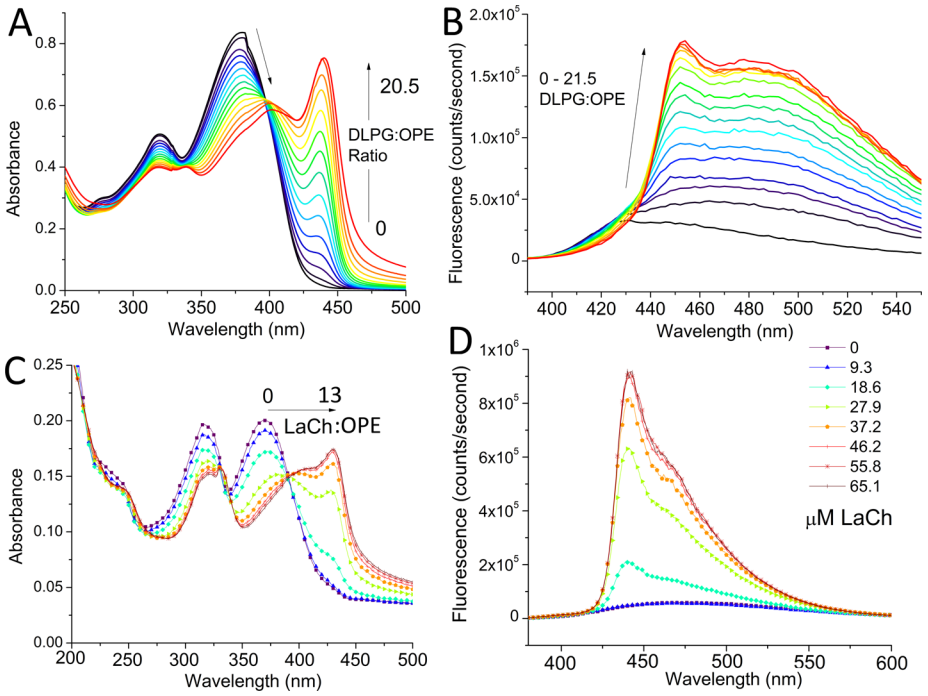

Figure 2. Absorbance and fluorescence spectra of (A) absorbance and (B) fluorescence (Ex, 375 nm) of 1.4 μM +2C with DLPG; (C) absorbance and (D) fluorescence (Ex, 370 nm) of 5 μM −1C with LaCh; all spectra indicate the varying DLPG/LaCh concentration or ratio of substrate to OPE.

2 mg/mL solution of LaCh is added and allowed to mix for several minutes. A similar procedure is followed for the preparation of the +2C/DLPG sensor. Typical sensors used in experiments with +2C/DLPG had concentrations of 1.4 μM OPE and DLPG concentrations of 16 μM. For the AChE sensor, 5 μM of −1C was used, and LaCh used for enzyme studies was 32 μM. Enzyme concentrations in the range of 50 to 0.5 mU were tested for PLA1 and PLA2, and the range for AChE was 0.1 to 0.8 U.

Absorbance and Fluorescence Spectroscopy. UV−visible absorption spectra were obtained using a Lambda-35 UV−vis Spectrometer fitted with a temperature-controlled cell with magnetic stirring (PerkinElmer, Waltham, MA). Fluorescence spectra were obtained using a Photon Technology International fluorescence spectrometer equipped with a 75 W xenon arc lamp housed in an elliptical reflector (Photon Technology International, Birmingham,NJ). Fluorescence quantum yields were calculated using the comparative method[46] relative to the previously reported value for +2C.[21] Least-squares linear regressions for substrate concentration calibration and fluorescence quantum yield determinations were performed using the software Origin 9.

Detection of Enzyme Activity. The monitoring of the sensor was performed using the absorbance wavelength of 430 nm and the fluorescence wavelength of 440 nm (excitation of 370 nm for −1C, 375 nm for +2C). For both absorbance and fluorescence measurements of the sensor upon addition of enzyme, the sensor was prepared as described above in a quartz cuvette with constant stirring at room temperature (25 °C). The lid of the instrument was quickly lifted and enzyme injected, resulting in a ∼0.5 s delay in the initial change registered. Enzyme kinetics were determined for PLA1 and PLA2 by converting the intensity of fluorescence or absorbance of the aggregate to substrate (DLPG) concentration, as given in eq 1 below.

$$[S]_t = [S]_0 \frac{\left(\frac{I_t}{I_b}\right) - 1}{\left(\frac{I_0}{I_b}\right) - 1} \quad (1)$$

Where $[S]_t$ denotes substrate concentration at time t, $[S]_0$ is initial substrate concentration, I_t is fluorescence intensity at time t, I_0 is initial fluorescence intensity, and I_b is background fluorescence intensity. Once the fluorescence at 440 nm or absorbance at 430 nm is converted to substrate concentration, standard Michaelis−Menten kinetics can be used. Nonlinear fitting to a velocity vs substrate concentration plot was performed using the Hill equation using Origin 9, with the formula given in eq 2. The Michaelis−Menten equation serves as a special example of the Hill equation, and when n = 1, the Hill equation is equivalent to the Michaelis−Menten equation commonly used for enzyme kinetics.[47]

$$y = \frac{V_{max} x^n}{(k_m^n + x^n)} \quad (2)$$

Where n = cooperativity, V_{max} is the max velocity in μmol/(min mg) or μM/min, and k_m is the substrate concentration at half of V_{max}.

Computational Methods. OPEs were parametrized to the generalized Amber force field (GAFF) framework using the antechamber program in AmberTools12.[48,49] The Lipid14 parameters for Amber were used for the lipid 1,2-dioleoyl-*sn*-glycero-3-phospho-1′-rac-glycerol (DOPG).[50] The Gaussian09 software package was used for all quantum-level calculations for residue parametrization, with geometry optimized at the B3LYP/6-31g** level and electrostatic potentials used for residue parametrization derived with Hartree−Fock and a 6-31g** basis set.[51] GAFF atomtypes were used to assign van der Waals parameters and bonding force constants.[49] The assigned partial charges of the OPE from the quantum-level calculations were fitted using the RESP charge fitting method.[52,53] The initial system configurations were prepared using the program Packmol.[54] Systems were solvated with water and neutralized with sodium and chloride ions, and the TIP3 water model was used.[55] Simulations used full PME electrostatics[56] and cubic periodic boundary conditions. The system was first minimized using the steepest descent method for 2500 steps, followed by a 250 step gradient minimization. Heating was carried out from 0 to 100 K in 500 ps, and then from 100 to 303.15 K in 500 ps using the NVT ensemble. Simulations were performed for 100−250 ns using the NPT ensemble with the Langevin barostat and thermostat with a time constant of 1/ps.[57,58] The Amber12-GPU software package was used with SPFP precision.[59,60] Radial distribution functions were measured over the simulation trajectory using the

DOI: 10.1021/acsami.5b00185
ACS Appl. Mater. Interfaces 2015, 7, 5550−5560

center of masses of the individual OPEs using the cpptraj program in AmberTools.[61] In order to sort out the most likely aggregated form of an OPE dimer, cpptraj was used to cluster interacting pairs of OPEs with the hierarchical agglomerative approach. The distance between frames was calculated using best-fit RMSD of the coordinates, and clustering analysis was carried out for OPEs within 5 Å apart. UCSF Chimera version 1.10 was used for rendering snapshots of the trajectories and further clustering of the trajectories of the top clustered results from cpptraj, based on pairwise best-fit root-mean-square deviations between separate OPEs, to distinguish common aggregate structures and provide a graphical representation of the clusters over time.[62]

RESULTS AND DISCUSSION

Photophysical Effects of Complex Formation. The fluorescence detection of enzyme activity on lipids or lauroyl choline was enabled by the strong photophysical changes which occurred upon aggregation of the OPEs. The changes in absorbance and fluorescence spectra of +2Cwith DLPG and −1C with LaCh are shown in Figure 2.

As can be seen in Figure 2, there are significant changes in the fluorescence and absorbance of aggregates of both anionic and cationic OPEs. Interestingly, the changes resulting from aggregation are very similar for the +2C/DLPG and −1C/LaCh complexes. The absorbance spectrum is strongly red-shifted, with the major transition moving from 375 to 440 nm. The minor band at ∼320 nm forms a bimodal shape with a second peak at 330 nm for −1C and 340 nm for +2C upon aggregation. In a solution of OPE with greater than 0.5 OD at λ_{max}, the formation of aggregates turns the solution from colorless and transparent to transparent yellow with a slight bluish haze. The blue haze is likely from the efficient fluorescence which occurs even under white fluorescent room lights. In addition to the strong changes to absorbance, the fluorescence is significantly altered upon aggregation with the substrate molecules. The most significant effect which can be utilized for sensing is a strong enhancement of fluorescence from a broadened, weak fluorescence to a very strong, structured emission centered at 455 nm for +2C and 442 nm for −1C.

The spectra in Figure 2 also show that both aggregates give rise to structured bands in both the absorbance and fluorescence spectra which are much closer in energy than in an unaggregated state (14 nm for +2C with DLPG, 10 nm for −1C with LaCh). This result shows that the fluorescence results in very little energy loss, giving a very active sensor. The red-shifted absorbance and enhanced fluorescence is typical of a "J-aggregate", which leads us to predict that the molecular structure that results in these enhanced electronic properties allows these rigid molecules to align. Comparing Figure 2B with Figure 2D it is clear that the −1C/LaCh aggregate has a more dominant structured band at ∼440 nm than the +2C/DLPG aggregate. This suggests that the structure of the −1C/LaCh aggregate is that of a well-defined J-dimer, where the +2C/DLPG aggregate likely is also a J-dimer but with more conformational freedom. This result of fluorescence enhancement suggests that the fluorescence quantum yields would be useful for describing the enhancement by the aggregation.

Fluorescence quantum yields were determined using the comparative method as discussed in the methods section, and the least-squares linear regressions of the results are given in Figure S1 of the Supporting Information. Figure S1 clearly demonstrates that the quantum yields of the OPEs are greatly enhanced by the aggregation induced by the substrates DLPG or LaCh. Calculation of the fluorescence yield by the comparative method using the reported value of 0.039 (±0.001) for +2C leads to vastly overstated quantum yields of fluorescence of both AChE and PLA sensors in excess of unity.[21] While it is understandable that the previous value of +2C was difficult to pinpoint due to the very low fluorescence of +2C in water, the results of fluorescence quantum yield measurements performed in this study suggest that the quantum yield for +2C is no larger than 0.016 rather than 0.039. This value would assume a quantum yield for the −1C/LaCh complex of near unity, and while the aggregation-induced fluorescence is extremely efficient, the quantum yield is likely between 0.9 and 1.0. The aggregation of +2C with DLPG results in a fluorescence enhancement 39 times at 440 nm, which correlates to an increase of fluorescence quantum yield from 0.016 ± 0.001 to 0.63 ± 0.03. The aggregation of −1C with LaCh results in a considerable enhancement of fluorescence quantum yield, which is 66 times higher for the −1C/LaCh complex than −1C alone. This correlates with an enhancement from 0.015 ± 0.002 to 0.98 ± 0.15, following the correction of the quantum yield of fluorescence of +2C from 0.039 to 0.016.

In addition to the strong changes in absorbance and fluorescence of the OPEs, the formation of a complex can be confirmed through circular dichroism (CD) spectroscopy. As can be seen in Figure S2 in the Supporting Information, +2C with DLPG strongly absorbs circularly polarized light with a strong negative band at 445 nm. Since DLPG is chiral, it is reasonable that an aggregate formed on a DLPG template would be optically active. The photophysical changes observed upon complexation allow for a variety of strategies for sensing the presence of a substrate. The aggregation with surfactants and substrates is useful, and the introduction of substrates that are degradable by enzymes allows us to use the OPEs as fluorescence-quenching enzyme sensors.

Molecular aggregates of these molecules have been reported before, and a comparison of the different studies gives insight into the structure of the aggregates depending on the scaffold which they are aggregated onto.[21−24] In a recent study, −1C was shown to form aggregates with the surfactant DTAB, however the structured high-energy fluorescence and low-energy absorbance typical of J-aggregates were not apparent, with a redshift of only 25 nm (compared with >70 nm in this study) and a fluorescence quenching effect rather than an enhancement.[22] Despite the similarities between DTAB and lauroyl choline, both of which are simple anionic surfactants, the aggregate formed between −1C and lauroyl choline gives rise to evidence of a more structured aggregate with more "J-type" character. In an earlier study, the aggregation of +2C was examined with the anionic cellulose derivative, carboxymethyl-cellulose.[21] The photophysical changes observed in that study were quite similar to those observed between +2C and DLPG in Figure 2A, B, with the only major difference being a lack of a structured peak at the λ_{max} of fluorescence of the aggregate. In a more recent study, the simple anionic surfactant sodium dodecyl sulfate was complexed with +2C, and the resulting photophysical changes were quite interesting; the absorbance changes were somewhat similar to what is shown in Figure 2A, but the fluorescence was strongly red-shifted from ∼450 to ∼530 nm, giving a visible transition from blue to green.[24] These previous studies give insight into the structure of the aggregates through similarities between photophysical properties of different systems. While no clear similarities were found in

DOI: 10.1021/acsami.5b00185
ACS Appl. Mater. Interfaces 2015, 7, 5550−5560

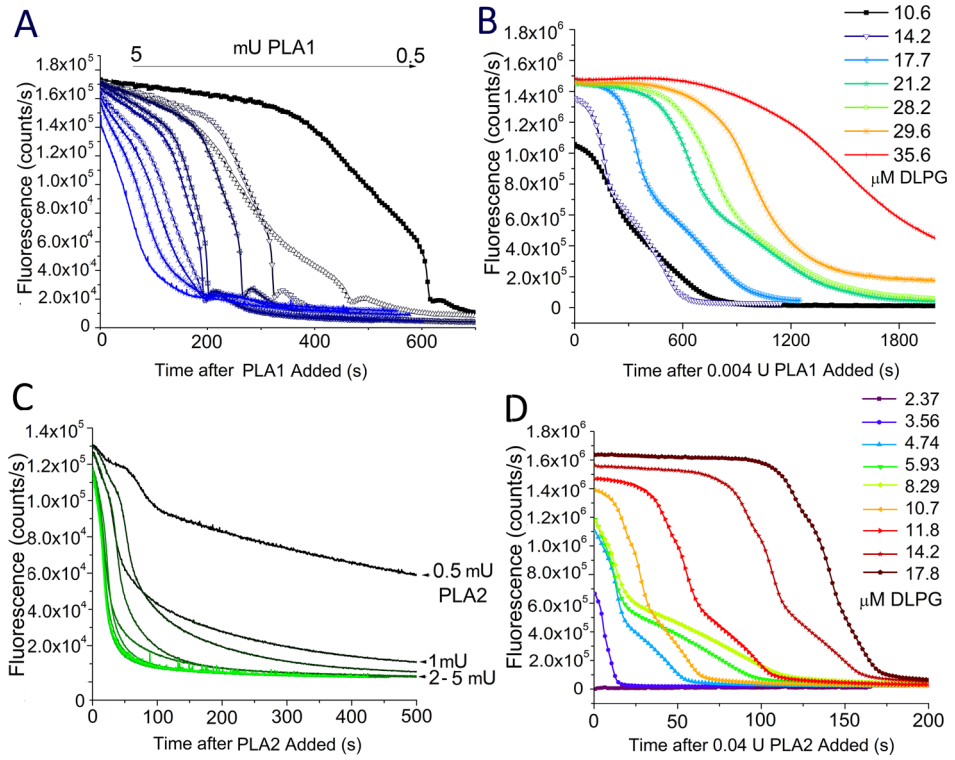

Figure 3. (A) Fluorescence of the +2C/DLPG aggregates over the course of PLA1 activity with 1.4 μM OPE and a DLPG concentration of 7.27 μM, with enzyme added ranging from 0.5 to 5 mU of PLA1. (B) 1.4 μM of +2C with DLPG at a series of concentrations from 10.6 to 35.6 μM (7.5−25.4 DLPG:OPE ratio), followed by addition of 4 mU of PLA1. (C) Fluorescence of the +2C/DLPG aggregates over the course of PLA2 activity with 1.4 μM OPE and a DLPG concentration of 7.27 μM, with enzyme added ranging from 0.5 to 5 mU of PLA2. (D) 1.4 μM of +2C with DLPG at a series of concentrations from 2.37 to 17.8 μM (1.7−12.7 DLPG:OPE ratio), followed by addition of 40 mU of PLA1. t = −1 s is the time of enzyme addition. Wavelength of excitation is 375 nm, emission is 440 nm.

studies with −1C, the aggregates observed with +2C/DLPG are very similar to those observed with +2C and carboxymethylcellulose (CMC). As CMC is a highly planar anionic scaffold, this leads to the hypothesis that the DLPG and possibly LaCh provides a planar environment or scaffold which promotes linear alignment of the backbones of the OPEs. A set of all-atom molecular simulations were performed to further investigate the structure of the aggregates, and the results are discussed following the experimental results below.

Molecular Aggregates for Monitoring Enzyme Activity: Phospholipases A1, A2, and C. The use of lipids such as DLPG to induce aggregation allows for the creation of a sensor that can be affected by phospholipases. Phospholipases are a class of phosphodiesterases that can cleave the acyl chains or phosphate groups of the lipids, as discussed in the introduction. The changes in absorbance and fluorescence of the +2C/DLPG complexes were monitored after addition of either PLA1, PLA2, or PLC to the solution as described in the methods section. In addition to varying enzyme concentration, a study varying the concentration of DLPG was also carried out to determine changes in the response rate of the sensor when excess lipid is present. The effects of enzymatic activity on the +2C/DLPG sensor are shown for PLA1 and PLA2 in Figure 3.

As can be seen in Figure 3, decomposition of the DLPG lipids by PLA1 and PLA2 results in swift quenching of the fluorescence. Although monitoring absorbance (see Figure 2A, C) can allow one to determine enzyme activity, enhanced fluorescence quenching and unquenching allows for a more sensitive sensor to be achieved through fluorescence monitoring. In Figure 3B, D, the effects of varying lipid concentration on the rate of enzymatic degradation was tested. In samples which had a lipid concentration higher than the saturation point of ∼1:16 OPE:lipid ratio, a lag period was observed after the addition of the enzyme. This lag period is tied to the amount of excess, "free" lipid in solution, as it increases with increasing lipid and constant OPE concentration. It is likely that there is a population of lipids which are circulating in solution without being involved in an aggregate with an OPE, and these lipids can act as a sort of "reserve" which can become involved in an aggregate if needed. The enzymes will also be acting on these free lipids, retarding the degradation of the OPE-Lipid sensor. Once this population of excess lipids is enzymatically cleaved by PLA1 or PLA2, the lipids making up the sensor are then cleaved and the fluorescence quenching occurs. Figures 3A and C demonstrate the high sensitivity of the phospholipase sensor, as enzymatic cleavage is observed with both PLA1 and PLA2 at enzyme concentrations below 5 mU/mL, which is the previously reported detection limit for PLC of a recently reported PPE-based PLC-sensor.[20] Since the weight of PLA1 from *T. lanuginosus* is not known, and the enzyme is obtained with concentration listed in terms of units of activity, it is difficult to compare PLA1 limits of detection on a molar basis. The concentration of PLA2 that corresponds with 0.5 mU/mL at 320 U/mg protein is 500 fM, marking at least a 10-fold increase in sensitivity over the previously reported PLC sensor.

In a previous study, by Liu and co-workers, a polymeric *p*-phenylene ethynylene with anionic side chains was used to detect phospholipase C activity after aggregation with a neutral lipid.[20] In an interesting turn, the activity of PLC does not result in a strong change to the sensors aggregated state. The

DOI: 10.1021/acsami.5b00185
ACS Appl. Mater. Interfaces 2015, 7, 5550−5560

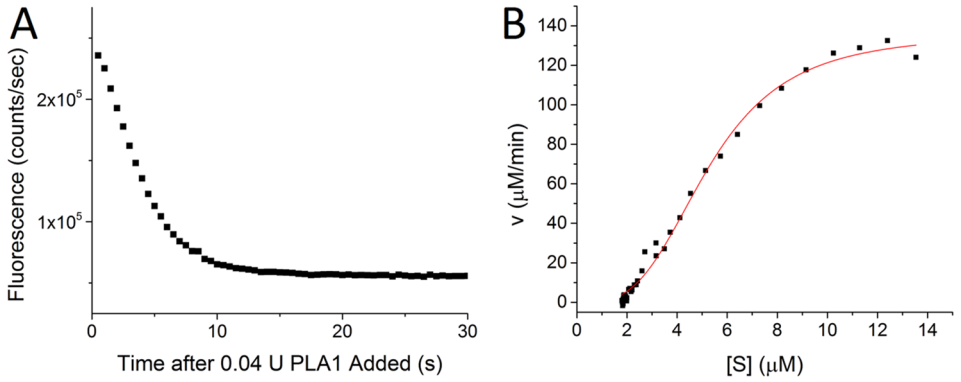

Figure 4. (A) Fluorescence of PLA sensor (Ex, 375 nm; Em, 440 nm) composed of 1.4 μM +2C and 16 μM DLPG following addition of 0.04U of PLA1. (B) Velocity versus substrate plot after conversion of data in A to velocity and substrate following the equations given in the methods section.

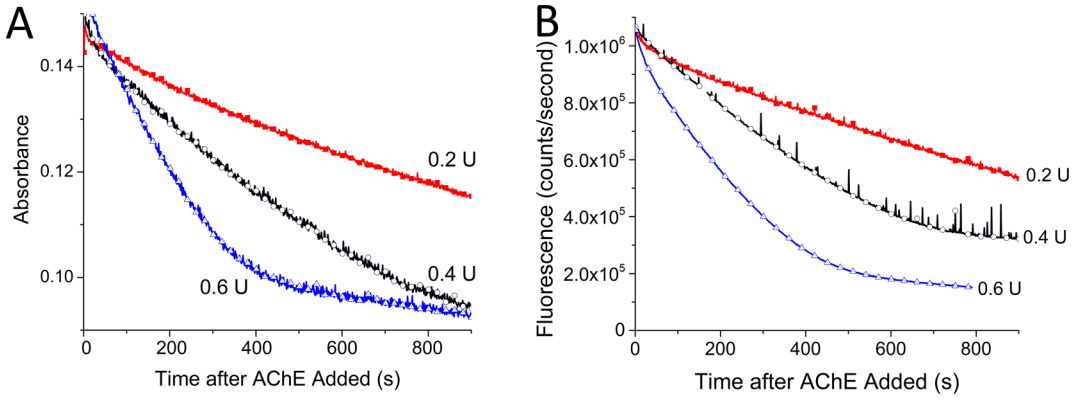

Figure 5. (A) Absorbance at 430 nm and (B) fluorescence (Ex, 370 nm; Em, 440 nm) of −1C and LaCh at 0.2, 0.4, and 0.6 U of AChE.

changes resulting from addition of PLC are shown in Figure S3 in the Supporting Information. It is clear that there is no fluorescence quenching or absorbance change after addition of PLC as was observed with PLA1 and PLA2. This behavior suggests that one or both of the products of PLC degradation, diacyl glycerol, and 1-lauroyl-*sn*-glycerol 3-phosphate, also result in aggregation of the OPE which allows retention of the enhanced fluorescence.

Monitoring Enzyme Kinetics: PLA Sensing. The difference between the aggregation of PLA and AChE sensors is further shown when one examines the kinetics of complex formation at different concentrations. The ability to quantify substrate concentration is afforded by these sensors, but only when substrate concentration can be effectively calculated from the fluorescence or absorbance of the aggregate. It is somewhat visible when comparing Figures 2A, B with Figures 2C, D that the increase of the absorbance (430 nm) or fluorescence peaks (440 nm) representing the aggregate changes with a different concentration dependence for the two sensors. This is better shown when one constructs calibration curves to fit fluorescence or absorbance to substrate (DLPG or LaCh) concentration. The linear correlation between fluorescence at 440 nm and substrate concentration is given for both PLA and AChE sensors in Figure S4 in the Supporting Information. The curves shown in Figure S4 in the Supporting Information illustrate a difference in the concentration dependence for formation of the PLA and AChE sensor. +2C shows a linear increase in fluorescence with increasing DLPG concentration, but −1C shows a sharp change with a typical sinusoidal shape between 20 and 30 μM of LaCh. The linear response of the PLA sensor is ideal for quantification of kinetic parameters, as the concentration of lipid can be calculated from the linear regression. Regrettably, the sinusoidal response of the AChE sensor does provide a linear fluorescence signal to LaCh concentration. This suggests that despite the similarities between the aggregates, the formation of the aggregates follows different kinetics. The kinetics of the degradation of the +2C/DLPG sensor by PLA1 and PLA2 were followed by conversion of the fluorescence or absorbance to concentration, as discussed in the methods section. An example of the result is given in Figure 4, where the loss of fluorescence over time is converted into velocity vs substrate concentration for calculating enzyme kinetics.

The activity of PLA1 and PLA2 were determined by nonlinear fitting of fluorescence or absorbance of the aggregated OPEs in the sensor by the Hill fit.[47] PLA1 from *T. lanuginosus* was found to have a V_{max} of 141.7 ± 6.8 μM/min, and a k_m of 5.41 ± 0.28. PLA2 from *C. adamanteus* venom had a V_{max} of 37.4 ± 1.84 μM/min and a k_m of 6.39 ±0.29. The specific activity of PLA2 was calculated using 0.05 U/mL of 320 U/mg PLA2 to be 1295 μmol min^{-1} mg^{-1}, nearly 1000-fold greater than the 14 μmol min^{-1} mg^{-1} obtained from a previous study of PLA2 from *C. atrox* venom.[63] For these sensors the km is tied to the OPE concentration, and in cases with PLA1, where the OPE concentration is 10 μM instead of 1.4 μM and the kM is 97 μM rather than 5.4. There was a strong correlation observed between increased substrate concentration and enzyme activity because of a cooperative effect. This is expressed as *n* in eq 2, which was fit to the results to determine kinetic parameters. In a case of no cooperativity, *n* is equal to

DOI: 10.1021/acsami.5b00185
ACS Appl. Mater. Interfaces 2015, 7, 5550−5560

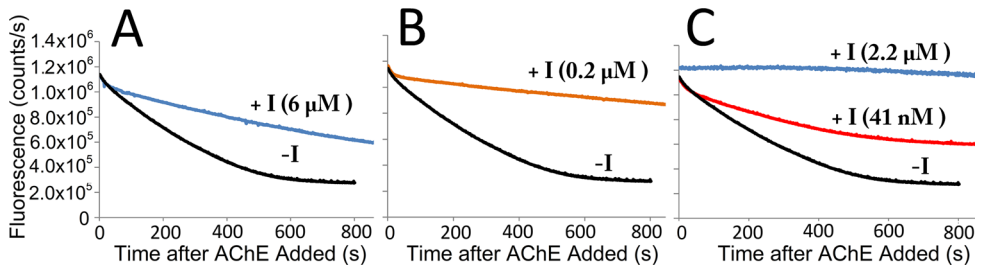

Figure 6. Fluorescence (λ_{exc} = 370 nm, λ_{em} = 440 nm) of −1C/LaCh complex (5 μM OPE, 32 μM LaCh) after addition of 0.6 U of AChE in the presence of AChE inhibitor (A) Itopride HCl, (B) Meptazinol HCl, and (C) TAE-1. Traces with inhibitor are denoted with +I and the inhibitor concentration, and −I indicates no inhibitor.

one, but for both PLA1 and PLA2 it is fit to be 3. The cooperative effect is visible in Figure 4, where there is a decreased slope of $v/[S]$ in regions of low substrate. This is reasonable, as PLA1 and PLA2 have been previously shown to be membrane-associated proteins that have activity that is highly dependent on the local lipid environment.[63,64]

Monitoring Enzyme Activity: Acetylcholinesterase. Acetylcholinesterase (AChE) is an important enzyme that is responsible for terminating synaptic transmission by hydrolyzing the neurotransmitter acetylcholine. As was discussed previously, the compound lauroyl choline was used instead of acetylcholine, as acetylcholine lacks a sufficient hydrocarbon tail to form an aggregate with the OPE. In addition to the absorbance and fluorescence spectra in Figure 2, the quantum yields were calculated to be near unity upon formation of aggregates between −1C and lauroyl choline. This highly sensitive fluorescence response in particular makes this an ideal sensor for detection of AChE. The detection of AChE by fluorescence and absorbance using the −1C/LaCh sensor is shown in Figure 5.

As shown in Figure 5, there is clear detection of AChE activity through the loss of the characteristic absorbance at 430 nm and fluorescence at 440 nm over time. There was a clear difference in the rate of enzymatic degradation of the complex which correlated with amount of enzyme added. In the absorbance spectrum (Figure 5A), there is a quick drop from 0.16 OD, and for the 0.4 and 0.2 Unit additions of AChE this rate progressively decreases, leading to a curve with a more gradual slope. The slope of the 430 nm absorbance loss after adding 0.6 Units of enzyme is fairly constant until 0.1 OD approaches, indicating that the aggregate has been dissociated. In Figure 5B, the fluorescence drops an order of magnitude from 1×10^6 to 1×10^5 photons/s, compared with a change from 0.16 to 0.1 OD for the change in absorbance at the same concentration.

As stated in the introduction, AChE is responsible for termination of nerve signals. This causes many inhibitors of AChE to be highly neurotoxic, and many pesticides and nerve agents are strong AChE inhibitors.[35] To determine whether the AChE sensor based on the −1C/LaCh complex could be used for detection of AChE inhibitors such as nerve agents and pesticides, the sensor was added to a solution of one of three different AChE inhibitors prior to addition of AChE. While the compounds; TAE-1, Itopride, and Meptazinol, all have been shown to be AChE inhibitors, these compounds are less volatile and toxic than the nerve agents and pesticides which are of primary interest for AChE inhibition detection. The inhibition of AChE by these three inhibitors using the −1C/LaCh sensor was carried out as described in the methods, and the fluorescence of the sensor over time with and without inhibitor is given in Figure 6.

As shown in Figure 6, inhibition of AChE by several different inhibitors is apparent by the attenuated loss of fluorescence compared with the reference solution with no inhibitor. To confirm that this result is not due to aggregation between the OPE and the inhibitors, the absorbance and fluorescence spectra of the OPE and inhibitor without LaCh were obtained. As shown in Figure S5 in the Supporting Information, there is no significant aggregation induced by Itopride or Meptazinol. TAE-1, however, does result in a red-shifted absorbance and a strongly red-shifted and broadened green fluorescence. Fortunately, there is little overlap between the fluorescence of the TAE-1/OPE complex and that of the OPE/LaCh complex, giving only a slight bias to the overall fluorescence.

Prediction of Aggregate Structure by Molecular Simulations. To study the structure of the aggregate formed between cationic OPEs and anionic phospholipids, we performed simulations with +1C and DOPG near the experimentally observed ratio of lipid:OPE using all-atom molecular dynamics. Although +2C was used primarily in this study, +1C was shown to form an aggregate resulting in similar photophysical changes (see Figure S6 in the Supporting Information). To reduce computational time, we used +1C in the simulations rather than +2C. The full details of the all-atom molecular dynamics simulations including atom number, system size, and simulation length, are given in Table S1 in the Supporting Information. It should be noted that the simulations where only 2 OPEs was used did not result in the formation of an aggregate within the 150 ns simulation time, as the two OPEs in the simulation never came close enough to interact with one another in this time. This was observed at both simulation box sizes used (8 or 10 nm side length), and with an OPE lipid ratio of 1:3 and 1:10. The aggregation of the different OPEs is followed through radial pair distribution functions based on the centers of mass of the two OPEs in Figure S7 in the Supporting Information. Timelines of the three simulations in which aggregation between OPEs was observed are given in Figure 7.

The aggregation of the OPEs is preceded by the formation of a micelle, as can be observed when comparing the first and second images of the timeline in Figure 7. This process was slower in the larger system with 42 lipids and a 10 nm box, and in this case several smaller micelles were formed initially which then agglomerated into larger micelles. The effect of the OPEs on the extent of lipid aggregation was analyzed by comparing the final size of lipid aggregates and radial pair distributions between lipid tails in simulations with 42 lipids and either 4 or no OPEs. The simulation including OPEs resulted in two

DOI: 10.1021/acsami.5b00185
ACS Appl. Mater. Interfaces 2015, 7, 5550−5560

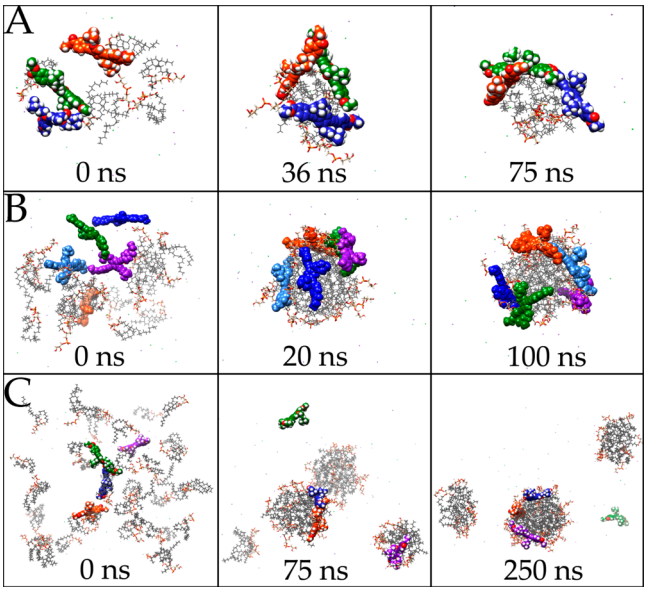

Figure 7. Snapshots of simulation trajectories for (A) 3 OPE, 6 DOPG, (B) 5 OPE, 20 DOPG, (C) 4 OPE, 42 DOPG. Lipid tails are colored gray, headgroups are colored red and orange, and OPEs are colored Orange, Blue, Purple, or Green to distinguish between them.

micelles, one with 25 lipids and one with 17, where the larger one had three OPEs at the interface and the smaller had only one. Without OPEs, the simulation also resulted in two micelles in a similar time frame, with one containing 23 lipids and one containing 19. The lipid number of ∼20 for these micelles that form in simulations of 42 lipids with and without OPEs may not increase, as the anionic headgroups of the DOPG are likely to repel one another once a stable micelle size is reached. The radial pair distributions calculated between the centers of mass of the oleyl chains of the lipids over the simulation show that there is only a slight increase in the extent of lipid aggregation with OPEs than without (Figure S8 in the Supporting Information). These results suggest that in the simulations there is no significant difference in the aggregation of the lipids in the presence of OPEs.

When more than 2 OPEs were simulated with the lipids the aggregation of OPEs was observed to shortly follow the formation of a micelle by the lipids. In the simulations with only two OPEs, there was not a significant amount of aggregation. The radial distribution functions in Figure S7 in the Supporting Information show that the aggregation of the OPEs increases following an increasing ratio of OPE to lipids in a micelle. Because the OPEs on the micelle are not interacting with other OPEs, the ratio of lipid:OPE is 1:2, 1:4, and 1:8.3 when only considering the micellar environment. The aggregates that occur at these different ratios and micelle sizes provides a thorough look at the different aggregate structures, and their dependence on micelle curvature or number of OPEs.

It is clear that aggregation is occurring on the surface of micellar lipid aggregates, but the all-atom simulation trajectories give only a fleeting glimpse into the OPE dimer structures since the system is dynamic. The most common forms of aggregated OPE dimers were determined by clustering via root-mean-squared distance between coordinates, which allowed rapid sifting of the results to obtain groupings of trajectory frames which correlate with specific aggregate structures. A summary of the clustering analysis and most likely structures for the three simulations in which molecular aggregates were formed is given in Figure 8.

The results of clustering analysis in Figure 8 show several dominate aggregate structures. The majority of aggregates formed on the ∼20 lipid micelles involved an OPE dimer with overlap of a single phenyl ring, and the backbones of the OPEs oriented at an oblique angle to one another, as represented by the cyan cluster in Figure 8. Loosely bound aggregates of a similar structure are shown in orange in Figure 8. In these more loosely bound aggregates, no overlap between phenyl rings is observed, only overlap between carboxyester termini. In the cases where the lipid aggregate is larger (Figure 8B, C), the aggregates do not form an aggregate with as sharp an angle

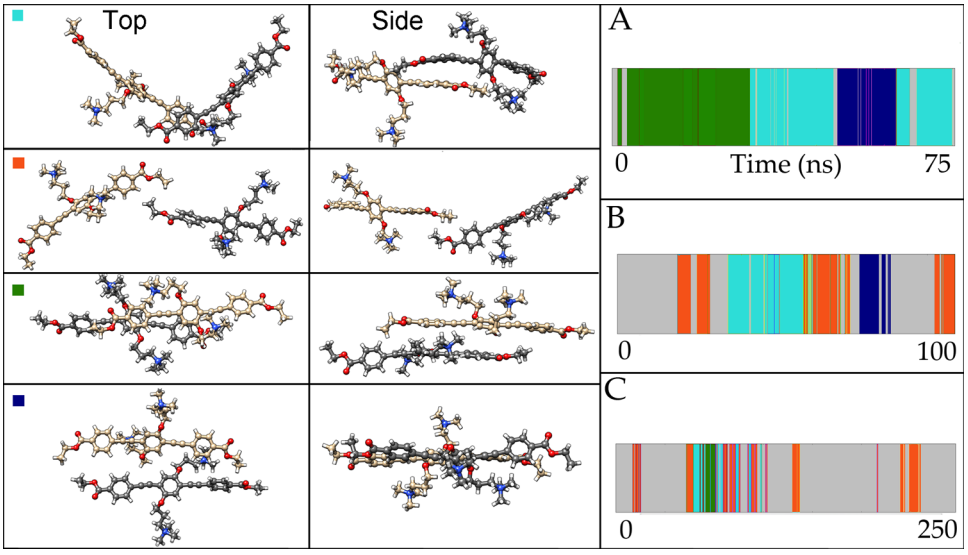

Figure 8. Representative structures of the top two clustered results from (A) 3 OPE, 6 DOPG (2:1 lipid:OPE), (B) 5 OPE, 20 DOPG (4:1 lipid:OPE), (C) 4 OPE, 42 DOPG (10.5:1 lipid:OPE), with clusters colored based on average structure. A colored square at the top-left of the top-view each structure denotes which cluster it belongs to in the graphs on the right, in which colors indicate different clustered aggregates. Gray color denotes OPEs that are unaggregated or in a loosely bound aggregate of more than 2 nm of separation.

DOI: 10.1021/acsami.5b00185
ACS Appl. Mater. Interfaces 2015, 7, 5550−5560

between them, due to decreased curvature of the micelle. The formation of edge−edge dimers was also observed, as shown in the navy blue cluster in Figure 8. Although this aggregate was not commonly observed compared with the end-end aggregates (cyan and orange), it lasted for a duration of at least 10 ns in the simulations in which it occurred (Figure 8A, B). Finally, a dimer with overlap of two phenyl rings on each molecule was found to occur in the beginning of the 6:3 lipid:OPE simulation, and is denoted with green (Figure 8A). This aggregate was present for only several nanoseconds in the 10.5:1 lipid:OPE simulation, which suggests that it plays only a minor role in the experimentally observed aggregation. This is reasonable, as this structure resembles a typical H-aggregate, which would not result in the photophysical properties that are experimentally observed.

The size of the lipid micelles does not appear to increase once a size of ∼20 lipids has been reached, because of the forces from electrostatic repulsion being greater than those from the free-energy associated with solvation of the lipid tails as the curvature becomes large enough. This computational result suggests that the experimentally observed linear increase in absorbance or fluorescence indicative of OPE aggregation may result from an increasing number of OPEs on a lipid micelle forming an extended aggregate. Because the simulations use DOPG, which has aliphatic chains that are 4 carbons longer than the experimentally studied DLPG, the size of ∼20 lipids for the aggregate may be larger than what occurs experimentally. The literature in this area is sparse; however, it has been shown that the presence of DLPG in a 1:9 ratio to dodecylphosphocholine depresseses the critical micelle concentration of from 1.5 to 0.5 mM.[65] The oblique nature of the aggregates that occur (Figures 7 and 8) are likely to result in the broadened, low-energy fluorescence that occurs in the +2C/DLPG aggregates.

The aggregation of multiple OPEs is suggested in the simulation with the highest OPE:lipid ratio (Figures 7A and 8A). The structure of this aggregate is similar to a herringbone-type aggregate, and takes the form of two of the oblique end-end dimers denoted as the cyan cluster in Figure 8 linked together.[66] The structure of this aggregate, which forms a cluster that lasts for the final 45 ns of the simulation shown in Figure 7A, is given in Figure S9 of the Supporting Information. In lipid micelles with multiple OPEs at the interface, this structure would likely give rise to the photophysical changes that are experimentally observed. The simulation results presented herein suggest that the molecular aggregates formed experimentally result from the formation of oblique dimers with a dominant end−end or edge−edge character on the surface of lipid clusters or micelles.

CONCLUSIONS

Oligo-*p*-phenylene ethynylenes with ionic pendant groups have been shown to be useful for sensing, and there is great interest in the ability to detect specific enzymes as biomarkers for pollution or disease. In this study, two sensors were formed by the noncovalent interactions between OPEs and oppositely charged substrates for target enzymes. These OPEs have carboxyester terminal groups which result in highly quenched fluorescence due to strong interactions with solvent, and have strongly enhanced fluorescence when in a water-poor environment. One sensor was formed between a cationic OPE and the phospholipid DLPG, and one was formed between an anionic OPE and the compound lauroyl choline, which contains acetylcholine. UV−visible spectroscopic methods were used to show that typical J-aggregates form between an anionic OPE and LaCh with a sigmoidal dependence on LaCh concentration, where the formation of +2C aggregates progressed linearly with DLPG concentration.

To gain a better understanding of the structure of the aggregates formed between the OPEs and the phospholipids, all-atom molecular dynamics simulations were carried out and the most common OPE dimer structure were extracted through clustering analysis. The results of the simulations show that the OPEs do indeed form aggregates on the lipid micelles which have a dominant end-end or edge−edge character. These results are consistent with experiment and shed a light on the interactions between the OPEs on the molecular level, in addition to providing a platform to study the effects of micelle size and curvature on the resulting structures of the aggregates. These simulations will serve as the basis for future density functional theory studies in order to compare the electronic structure and spectra of the aggregates with what is experimentally observed.

The sensor formed with DLPG was used to detect the activity of phospholipases A1 and A2, which caused a strong fluorescence quenching and loss of the 430 nm absorption band. Though a previous study showed that a PPE complexed with anionic lipids as an enzyme sensor was able to specifically sense phospholipase C, this enzyme had no effect on the +2C/DLPG sensor. The linear response of this sensor to substrate concentration allowed the use of standard Michaelis−Menten kinetics to calculate kinetic parameters of the enzymes, though a specific activity for PLA1 was not obtained because of lack of a known molecular weight of the specific enzyme from *T. lanuginosus*. The sensor formed from the aggregation of an anionic OPE with lauroyl choline was used to detect the activity of Human acetylcholinesterase. This sensor was able to not only detect the activity of the enzyme but sense inhibition of the enzyme through a study of three different AChE inhibitors. The results presented herein reinforce the use of phenylene ethynylene oligomers in the preparation of chemical and biological sensors with high sensitivity and selectivity, with applications in detection of disease biomarkers, environmental pollutants, or weaponized toxins.

ASSOCIATED CONTENT

Supporting Information

Simulation details, radial pair distributions, additional UV−visible and circular dichroism spectra mentioned in the text, plots used for fluorescence yield calculations, and additional aggregate structures. This material is available free of charge via the Internet at http://pubs.acs.org

AUTHOR INFORMATION

Corresponding Author

*E-mail: whitten@unm.edu.

Author Contributions

E.H.H. performed writing, experiments, and computational studies. Y.Z. performed experiments. D.G.W. and D.G.E. served in an advisory capacity.

Notes

The authors declare no competing financial interest.

DOI: 10.1021/acsami.5b00185
ACS Appl. Mater. Interfaces 2015, 7, 5550−5560

■ ACKNOWLEDGMENTS

We thank the U.S. Defense Threat Reduction Agency for support through grant HDTRA1- 08-1-0053, the U.S. National Science Foundation for support through grant DMR-1207362, the University of New Mexico Office Of Graduate Studies for support of E.H.H. via an Excellence Fellowship, and the UNM Center for Advanced Research Computing (CARC) for providing access to Gaussian09 software for support of the computational studies.

■ REFERENCES

(1) Altintas, Z.; Tothill, I. Biomarkers and Biosensors for the Early Diagnosis of Lung Cancer. *Sens. Actuators, B* **2013**, *188*, 988−998.
(2) Pandey, S.; Singh, A.; Dubey, A. P.; Mishra, T. K.; Kapoor, S. Estimation of Biomarkers Chitotriosidase and CCL18/PARC in Gaucher Patients: Indian Experience. *Indian J. Clin. Biochem.* **2014**, 1−5.
(3) Ramos, D.; Martins, E. G.; Viana-Gomes, D.; Casimiro-Lopes, G.; Salerno, V. P. Biomarkers of Oxidative Stress and Tissue Damage Released by Muscle and Liver after a Single Bout of Swimming Exercise. *Appl. Physiol. Nutr. Metab.* **2013**, *38*, 507−511.
(4) Abildgaard, U.; Heimdal, K. Pathogenesis of the Syndrome of Hemolysis, Elevated Liver Enzymes, and Low Platelet Count (HELLP): a Review. *Eur. J. Obstet. Gynecol. Reprod. Biol.* **2013**, *166*, 117−123.
(5) Vilella, F.; Ramirez, L.; Berlanga, O.; Martinez, S.; Alama, P.; Meseguer, M.; Simon, C. PGE2 and PGF2α Concentrations in Human Endometrial Fluid as Biomarkers for Embryonic Implantation. *J. Clin. Endocrinol. Metab.* **2013**, *98*, 4123−4132.
(6) Antoine, D. J.; Lewis, P. S.; Goldring, C. E.; Park, B. K. Are We Closer to Finding Biomarkers for Identifying Acute Drug-induced Liver Injury? *Biomarkers Med.* **2013**, *7*, 383−386.
(7) Altintas, Z.; Tothill, I. Biomarkers and Biosensors for the Early Diagnosis of Lung Cancer. *Sens. Actuators, B* **2013**, *188*, 988−998.
(8) Parnetti, L.; Castrioto, A.; Chiasserini, D.; Persichetti, E.; Tambasco, N.; El-Agnaf, O.; Calabresi, P. Cerebrospinal Fluid Biomarkers in Parkinson Disease. *Nat. Rev. Neurol.* **2013**, *9*, 131−140.
(9) Rostami, R.; Aghasi, M. R.; Mohammadi, A.; Nourooz-Zadeh, J. Enhanced Oxidative stress in Hashimoto's Thyroiditis: Inter-relationships to Biomarkers of Thyroid Function. *Clin. Biochem.* **2013**, *46*, 308−312.
(10) Shao, Y.; Wang, J.; Wu, H.; Liu, J.; Aksay, I. A.; Lin, Y. Graphene based Electrochemical Sensors and Biosensors: a Review. *Electroanalysis* **2010**, *22*, 1027−1036.
(11) Jacobs, C. B.; Peairs, M. J.; Venton, B. J. Review: Carbon Nanotube based Electrochemical Sensors for Biomolecules. *Anal. Chim. Acta* **2010**, *662*, 105−127.
(12) Vashist, S. K.; Zheng, D.; Al-Rubeaan, K.; Luong, J. H.; Sheu, F. S. Advances in Carbon Nanotube based Electrochemical Sensors for Bioanalytical Applications. *Biotechnol. Adv.* **2011**, *29*, 169−188.
(13) Pinto, M. R.; Schanze, K. S. Amplified Fluorescence Sensing of Protease Activity with Conjugated Polyelectrolytes. *Proc. Natl. Acad. Sci. U.S.A.* **2004**, *101*, 7505−7510.
(14) Feng, F.; Liu, L.; Yang, Q.; Wang, S. Water-Soluble Conjugated Polymers for Fluorescent-Enzyme Assays. *Macromol. Rapid Commun.* **2010**, *31*, 1405−1421.
(15) Li, K.; Liu, B. Water-soluble Conjugated Polymers as the Platform for Protein Sensors. *Polym. Chem.* **2010**, *1*, 252−259.
(16) Golub, E.; Niazov, A.; Freeman, R.; Zatsepin, M.; Willner, I. Photoelectrochemical Biosensors Without External Irradiation: Probing Enzyme Activities and DNA Sensing Using Hemin/G-Quadruplex-Stimulated Chemiluminescence Resonance Energy Transfer (CRET) Generation of Photocurrents. *J. Phys. Chem. C* **2012**, *116*, 13827−13834.
(17) Ji, X.; Yao, Y.; Li, J.; Yan, X.; Huang, F. A Supramolecular Cross-linked Conjugated Polymer Network for Multiple Fluorescent Sensing. *J. Am. Chem. Soc.* **2012**, *135*, 74−77.
(18) Dai, N.; Kool, E. T. Fluorescent DNA-based Enzyme Sensors. *Chem. Soc. Rev.* **2011**, *40*, 5756−5770.
(19) Zhou, Z.; Corbitt, T. S.; Parthasarathy, A.; Tang, Y.; Ista, L. K.; Schanze, K. S.; Whitten, D. G. End-Only" Functionalized Oligo-(phenylene ethynylene)s: Synthesis, Photophysical and Biocidal Activity. *J. Phys. Chem. Lett.* **2010**, *1*, 3207−3212.
(20) Liu, Y.; Ogawa, K.; Schanze, K. S. Conjugated Polyelectrolytes as Fluorescent Sensors. *J. Photochem. Photobiol., C* **2009**, *10*, 173−190.
(21) Tang, Y.; Hill, E. H.; Zhou, Z.; Evans, D. G.; Schanze, K. S.; Whitten, D. G. Synthesis, Self-assembly, and Photophysical Properties of Cationic Oligo(*p*-phenyleneethynylene)s. *Langmuir* **2011**, *27*, 4945−4955.
(22) Hill, E. H.; Sanchez, D.; Evans, D. G.; Whitten, D. G. Structural Basis for Aggregation Mode of oligo-*p*-Phenylene Ethynylenes with Ionic Surfactants. *Langmuir* **2013**, *29*, 15732−15737.
(23) Hill, E. H.; Zhang, Y.; Whitten, D. G. Aggregation of Cationic *p*-phenylene ethynylenes on Laponite Clay in Aqueous Dispersions and Solid Films. *J. Colloid Interface Sci.* **2014**, DOI: 10.1016/j.jcis.2014.12.006.
(24) Hill, E. H.; Evans, D. G.; Whitten, D. G. The Influence of Structured Interfacial Water on the Photoluminescence of Carboxyester-terminated Oligo-*p*-Phenylene Ethynylenes. *J. Phys. Org. Chem.* **2014**, *27*, 252−257.
(25) Qureshi, A.; Gurbuz, Y.; Niazi, J. H. Biosensors for Cardiac Biomarkers Detection: a Review. *Sens. Actuators, B* **2012**, *171*, 62−76.
(26) Packard, C. J.; O'Reilly, D. S.; Caslake, M. J.; McMahon, A. D.; Ford, I.; Cooney, J.; Lowe, G. D. Lipoprotein-associated Phospholipase A2 as an Independent Predictor of Coronary Heart Disease. *N. Engl. J. Med.* **2000**, *343*, 1148−1155.
(27) Ballantyne, C. M.; Hoogeveen, R. C.; Bang, H.; Coresh, J.; Folsom, A. R.; Heiss, G.; Sharrett, A. R. Lipoprotein-associated Phospholipase A2, High-sensitivity C-reactive Protein, and Risk for Incident Coronary Heart Disease in Middle-aged Men and Women in the Atherosclerosis Risk in Communities (ARIC) Study. *Circulation* **2004**, *109*, 837−842.
(28) Hurt-Camejo, E.; Camejo, G.; Peilot, H.; Öörni, K.; Kovanen, P. Phospholipase A2 in Vascular Disease. *Circ. Res.* **2001**, *89*, 298−304.
(29) Sudhir, K. Lipoprotein-associated Phospholipase A2, a Novel Inflammatory Biomarker and Independent Risk Predictor for Cardiovascular Disease. *J. Clin. Endocrinol. Metab.* **2005**, *90*, 3100−3105.
(30) Mallat, Z.; Lambeau, G.; Tedgui, A. Lipoprotein-Associated and Secreted Phospholipases A2 in Cardiovascular Disease Roles as Biological Effectors and Biomarkers. *Circulation* **2010**, *122*, 2183−2200.
(31) Packard, C. J. Lipoprotein-associated Phospholipase A2 as a Biomarker of Coronary Heart Disease and a Therapeutic Target. *Curr. Opin. Cardiol.* **2009**, *24*, 358−363.
(32) Torres, M. A.; Barros, M. P.; Campos, S. C.; Pinto, E.; Rajamani, S.; Sayre, R. T.; Colepicolo, P. Biochemical Biomarkers in Algae and Marine Pollution: a Review. *Ecotoxicol. Environ. Saf.* **2008**, *71*, 1−15.
(33) Carvalho, S. M.; Belzunces, L. P.; Carvalho, G. A.; Brunet, J. L. Badiou-Beneteau, A. Enzymatic Biomarkers as Tools to Assess Environmental Quality: A Case Study of Exposure of the Honeybee Apis mellifera to Insecticides. *Environ. Toxicol. Chem.* **2013**, *32*, 2117−2124.
(34) Rickwood, C. J.; Galloway, T. S. Acetylcholinesterase Inhibition as a Biomarker of Adverse Effect: a Study of Mytilus edulis Exposed to the Priority Pollutant Chlorfenvinphos. *Aquat. Toxicol.* **2004**, *67*, 45−56.
(35) Strelitz, J.; Engel, L. S.; Keifer, M. C. Blood Acetylcholinesterase and Butyrylcholinesterase as Biomarkers of Cholinesterase Depression among Pesticide Handlers. *Occup. Environ. Med.* **2014**, *71*, 842−847.
(36) Mdegela, R. H.; Mosha, R. D.; Sandvik, M.; Skaare, J. U. Assessment of Acetylcholinesterase Activity in Clarias gariepinus as a Biomarker of Organophosphate and Carbamate Exposure. *Ecotoxicology* **2010**, *19*, 855−863.
(37) Lionetto, M. G.; Caricato, R.; Calisi, A.; Giordano, M. E.; Schettino, T. Acetylcholinesterase as a Biomarker in Environmental

DOI: 10.1021/acsami.5b00185
ACS Appl. Mater. Interfaces 2015, 7, 5550−5560

and Occupational Medicine: New Insights and Future Perspectives. *BioMed. Res. Int.* **2013**, *2013*, 1−8.
(38) Pundir, C. S.; Chauhan, N. Acetylcholinesterase Inhibition-based Biosensors for Pesticide Determination: A Review. *Anal. Biochem.* **2012**, *429*, 19−31.
(39) Payne, J. F.; Mathieu, A.; Melvin, W.; Fancey, L. L. Acetylcholinesterase, an Old Biomarker with a New Future? Field Trials in Association with Two Urban Rivers and a Paper Mill in Newfoundland. *Mar. Pollut. Bull.* **1996**, *32*, 225−231.
(40) Hall, R. J.; Shenkin, S. D.; MacLullich, A. M. A Systematic Literature Review of Cerebrospinal Fluid Biomarkers in Delirium. *Dementia Geriatr. Cognit. Disord.* **2011**, *32*, 79−93.
(41) Shenhar-Tsarfaty, S.; Berliner, S.; Bornstein, N. M.; Soreq, H. Cholinesterases as Biomarkers for Parasympathetic Dysfunction and Inflammation-related Disease. *J. Mol. Neurosci.* **2013**, *53*, 298−305.
(42) Henry, M. S.; Passmore, A. P.; Todd, S.; McGuinness, B.; Craig, D.; Johnston, J. A. The Development of Effective Biomarkers for Alzheimer's Disease: a Review. *Int. J. Geriatr. Psychiatry* **2013**, *28*, 331−340.
(43) Birks, J. Cholinesterase Inhibitors for Alzheimer's Disease. *Cochrane Database Syst. Rev.* **2006**, CD005593.
(44) Sinha, N.; Firbank, M.; O'Brien, J. T. Biomarkers in Dementia with Lewy Bodies: a Review. *Int. J. Geriatr. Psychiatry* **2012**, *27*, 443−453.
(45) Tan, C.; Pinto, M. R.; Schanze, K. S. Photophysics, Aggregation and Amplified Quenching of a Water-soluble poly(Phenylene ethynylene). *Chem. Commun.* **2002**, 446−447.
(46) Williams, A. T. R.; Winfield, S. A.; Miller, J. N. Relative Fluorescence Quantum Yields using a Computer-controlled Luminescence Spectrometer. *Analyst* **1983**, *108*, 1067−1071.
(47) Goutelle, S.; Maurin, M.; Rougier, F.; Barbaut, X.; Bourguignon, L.; Ducher, M.; Maire, P. The Hill Equation: a Review of its Capabilities in Pharmacological Modelling. *Fundam. Clin. Pharmacol.* **2008**, *22*, 633−648.
(48) Case, D.A.; Babin, V.; Berryman, J.T.; Betz, R.M.; Cai, Q.; Cerutti, D.S.; Cheatham, T. E., III; Darden, T.A.; Duke, R.E.; Gohlke, H.; Goetz, A.W.; Gusarov, S.; Homeyer, N.; Janowski, P.; Kaus, J.; I. Kolossváry, Kovalenko, A.; Lee, T.S.; LeGrand, S.; Luchko, T.; Luo, R.; Madej, B.; Merz, K.M.; Paesani, F.; Roe, D.R.; Roitberg, A.; Sagui, C.; R. Salomon-Ferrer, Seabra, G.; Simmerling, C.L.; Smith, W.; Swails, J.; Walker, R.C.; Wang, J.; Wolf, R.M.; Wu, X.; Kollman, P.A. *AMBER 14*; University of California: San Francisco, 2014.
(49) Wang, J.; Wolf, R. M.; Caldwell, J. W.; Kollman, P. A.; Case, D. A. Development and Testing of a General AMBER Force Field. *J. Comput. Chem.* **2004**, *25*, 1157−1174.
(50) Dickson, C. J.; Madej, B. D.; Skjevik, A. A.; Betz, R. M.; Teigen, K.; Gould, I. R.; Walker, R. C. Lipid14: The Amber Lipid Force Field. *J. Chem. Theory Comput.* **2014**, *10*, 865−879.
(51) Frisch, M. J.; Trucks, G. W.; Schlegel, H. B.; Scuseria, G. E.; Robb, M. A.; Cheeseman, J. R.; Scalmani, G.; Barone, V.; Mennucci, B.; Petersson, G. A.; Nakatsuji, H.; Caricato, M.; Li, X.; Hratchian, H. P.; Izmaylov, A. F.; Bloino, J.; Zheng, G.; Sonnenberg, J. L.; Hada, M.; Ehara, M.; Toyota, K.; Fukuda, R.; Hasegawa, J.; Ishida, M.; Nakajima, T.; Honda, Y.; Kitao, O.; Nakai, H.; Vreven, T.; Montgomery, Jr., J. A.; Peralta, J. E.; Ogliaro, F.; Bearpark, M.; Heyd, J. J.; Brothers, E.; Kudin, K. N.; Staroverov, V. N.; Kobayashi, R.; Normand, J.; Raghavachari, K.; Rendell, A.; Burant, J. C.; Iyengar, S. S.; Tomasi, J.; Cossi, M.; Rega, N.; Millam, J. M.; Klene, M.; Knox, J. E.; Cross, J. B.; Bakken, V.; Adamo, C.; Jaramillo, J.; Gomperts, R.; Stratmann, R. E.; Yazyev, O.; Austin, A. J.; Cammi, R.; Pomelli, C.; Ochterski, J. W.; Martin, R. L.; Morokuma, K.; Zakrzewski, V. G.; Voth, G. A.; Salvador, P.; Dannenberg, J. J.; Dapprich, S.; Daniels, A. D.; Farkas, Ö.; Foresman, J. B.; Ortiz, J. V.; Cioslowski, J.; Fox, D. J. *Gaussian 09*, Revision C.1; Gaussian, Inc., Wallingford CT, 2009.
(52) Bayly, C. I.; Cieplak, P.; Cornell, W.; Kollman, P. A. A Well-behaved Electrostatic Potential based Method using Charge Restraints for Deriving Atomic Charges: the RESP Model. *J. Phys. Chem.* **1993**, *97*, 10269−10280.
(53) Cieplak, P.; Cornell, W. D.; Bayly, C.; Kollman, P. A. Application of the Multimolecule and Multiconformational RESP Methodology to Biopolymers: Charge Derivation for DNA, RNA, and Proteins. *J. Comput. Chem.* **1995**, *16*, 1357−1377.
(54) Martínez, L.; Andrade, R.; Birgin, E. G.; Martínez, J. M. PACKMOL: A Package for Building Initial Configurations for Molecular Dynamics Simulations. *J. Comput. Chem.* **2009**, *30*, 2157−2164.
(55) Jorgensen, W. L.; Chandrasekhar, J.; Madura, J. D.; Impey, R. W.; Klein, M. L. Comparison of Simple Potential Functions for Simulating Liquid Water. *J. Chem. Phys.* **1983**, *79*, 926.
(56) Darden, T. A.; York, D.; Pedersen, L. G. Particle mesh Ewald: An N• log(N) Method for Ewald Sums in Large Systems. *J. Chem. Phys.* **1993**, *98*, 10089−10092.
(57) Martyna, G. J.; Tobias, D. J.; Klein, M. L. Constant Pressure Molecular Dynamics Algorithms. *J. Chem. Phys.* **1994**, *101*, 4177−4189.
(58) Feller, S. E.; Zhang, Y.; Pastor, R. W.; Brooks, B. R. Constant Pressure Molecular Dynamics Simulation: The Langevin Piston Method. *J. Chem. Phys.* **1995**, *103*, 4613−4621.
(59) Salomon-Ferrer, R.; Goetz, A. W.; Poole, D.; Le Grand, S.; Walker, R. C. Routine Microsecond Molecular Dynamics Simulations with AMBER - Part II: Particle Mesh Ewald. *J. Chem. Theory Comput.* **2013**, *9*, 3878−3888.
(60) Le Grand, S.; Goetz, A. W.; Walker, R. C. SPFP: Speed without Compromise - a Mixed Precision Model for GPU Accelerated Molecular Dynamics Simulations. *Comput. Phys. Commun.* **2013**, *184*, 374−380.
(61) Roe, D. R.; Cheatham, T. E.; PTRAJ, I. I. I. and CPPTRAJ: Software for Processing and Analysis of Molecular Dynamics Trajectory Data. *J. Chem. Theory Comput.* **2013**, *9*, 3084−3095.
(62) Pettersen, E. F.; Goddard, T. D.; Huang, C. C.; Couch, G. S.; Greenblatt, D. M.; Meng, E. C.; Ferrin, T. E. UCSF Chimera–a Visualization System for Exploratory Research and Analysis. *J. Comput. Chem.* **2004**, *25*, 1605−1617.
(63) Yuan, W.; Quinn, D. M.; Sigler, P. B.; Gelb, M. H. Kinetic and Inhibition Studies of Phospholipase A2 with Short-chain Substrates and Inhibitors. *Biochemistry* **1990**, *29*, 6082−6094.
(64) Richmond, G. S.; Smith, T. K. Phospholipases A1. *Int. J. Mol. Sci.* **2011**, *12*, 588−612.
(65) Otzen, D. E.; Blans, K.; Wang, H.; Gilbert, G. E.; Rasmussen, J. T. Lactadherin Binds to Phosphatidylserine-containing Vesicles in a Two-step Mechanism Sensitive to Vesicle Size and Composition. *Biochim. Biophys. Acta, Biomembr.* **2012**, *1818*, 1019−1027.
(66) Spano, F. C. Excitons in Conjugated Oligomer Aggregates, Films, and Crystals. *Annu. Rev. Phys. Chem.* **2006**, *57*, 217−243.

DOI: 10.1021/acsami.5b00185
ACS Appl. Mater. Interfaces 2015, 7, 5550−5560